Morphology Development in Amorphous Polymer:Fullerene Photovoltaic Blend Films During Solution Casting

Andrew J. Pearson, Tao Wang, Alan D. F. Dunbar, Hunan Yi, Darren C. Watters, David M. Coles, Paul A. Staniec, Ahmed Iraqi, Richard A. L. Jones, and David G. Lidzey**

The evolution of film structure is reported during solution casting of PCDTBT:$PC_{70}BM$ 1:4 wt%, a polymer:fullerene blend system that finds application in an organic photovoltaic device. Using the complimentary techniques of grazing-incidence wide-angle X-ray scattering and spectroscopic ellipsometry, a number of distinct processes that occur during film formation are identified. This includes the growth of fullerene molecules into nanoscale aggregates, the onset of which coincides with the solubility limit of the material in the casting solvent being reached. An apparent delay in Bragg scatter from the PCDTBT-rich phase of the film suggests that, for the film composition studied here, the aggregation of $PC_{70}BM$ precedes weak self-organisation of the conjugated polymer. This behaviour is compared with the drying dynamics of a number of different polymer:fullerene blends that each contain a high weight fraction of fullerene molecules, and a range of comparable solid concentrations are identified beyond which the precipitation of fullerene aggregates from solution occurs. These observations provide an insight into the development of structure in relatively amorphous polymer:fullerene blends for organic photovoltaic applications and potentially assists the future optimisation of this category of materials.

1. Introduction

The ability to process photovoltaic devices using solution-based techniques is an attractive proposition[1,2] owing to the potential for such devices to be manufactured over large areas at low cost.[3] Organic photovoltaic (OPV) devices are one category of solution processable photovoltaics that have seen a rapid rise in power conversion efficiency (PCE)[4,5] and operating lifetime[6] in recent years, bringing the technology closer to the specifications deemed necessary for commercial viability.[7,8] The photoactive semiconducting layer within these devices is typically composed of a blend of a conjugated polymer and a functionalised fullerene, forming a self-assembled bulk-heterojunction (BHJ) architecture. In addition to the electronic properties of the constituent semiconductors, the structure of the BHJ has been demonstrated to significantly influence the efficiency of photocurrent generation.[9–12] It is presently believed that BHJ films are characterised by a partially phase separated nanoscale morphology, with co-existing regions of pure polymer, pure fullerene and a mixed polymer/fullerene phase all being present.[13–16] Efficient OPVs are in general characterised by structures that exist over a series of length-scales, including organisation at molecular length-scales and the formation of nanoscale percolated networks, with each length-scale having an important influence on the processes of photocurrent generation and charge extraction. To optimise BHJ morphology and create an OPV device having a high PCE requires control over many different parameters, including the choice of solvent, the conditions of film casting and the possible application of post-film deposition techniques.

Several studies[17–25] have applied a range of techniques to probe the formation and evolution of morphology in polymer:fullerene blend films during various stages in their preparation, drying and post processing in order to gain insight into the dynamic mechanisms that drive morphology evolution.[26] In addition to an improved physical understanding of such processes, the information obtained is likely to be of significant importance if such materials and devices undergo commercialisation and manufacture, as real-time process control will be a critical requirement. To date, the majority of

Dr. A. J. Pearson, Dr. T. Wang, D. C. Watters,
Dr. D. M. Coles, Prof. R. A. L. Jones, Prof. D. G. Lidzey
Department of Physics & Astronomy
University of Sheffield
Hicks Building, Hounsfield Road, Sheffield, S3 7RH, UK
E-mail: a.j.pearson@sheffield.ac.uk;
d.g.lidzey@sheffield.ac.uk
Dr. A. D. F. Dunbar
Department of Chemical and Biological Engineering
The University of Sheffield
Sir Robert Hadfield Building
Mappin St, Sheffield, S1 3JD, UK
Dr. H. Yi, Dr. A. Iraqi
Department of Chemistry
University of Sheffield
Sheffield, S3 7HF, UK
Dr. P. A. Staniec
Diamond Light Source Ltd
Diamond House
Harwell Science and Innovation Campus
Didcot, Oxfordshire, OX11 ODE, UK

DOI: 10.1002/adfm.201301922

such studies have addressed semi-crystalline polymer:fullerene blends and have observed a multi-step process of film formation toward a bulk-heterojunction morphology. These studies have provided insight to the underlying physical mechanism for phase separation in polymer:fullerene BHJ blends, with several reports of polymer crystallisation providing the dominant driving force for morphology formation rather than spinodal decomposition.[18,22,27–30] Whether crystallisation of either the polymer or fullerene component drives morphology formation however remains a topic of active research. Phase separation via crystallisation is likely to be triggered by either the polymer or fullerene depending on the following factors: the relative crystallinity of each material, their relative composition in a blend and the casting solvent used (including whether additives are used). The intentional pre-aggregation of either polymer or fullerene in solution will also have a significant influence on the kinetics of film formation. In polymer:fullerene blend films subject to thermal annealing or solvent vapour annealing, phase separation in initially well-mixed films can be initiated by the crystallisation of either polymer or fullerene. In these instances the exact composition of the film,[19] the annealing temperature (for thermal annealing) and choice of solvent vapour (for solvent annealing)[25] will all play an important role in the modifcation of film morphology. All these factors highlight the large and complex 'parameter-space' that exists in relation to morphology formation and evolution in polymer:fullerene blend thin-films.[26,27]

In this work, we investigate film structure formation in a predominantly amorphous polymer:fullerene blend film during solution casting. Structure formation is determined simultaneously using the complimentary techniques of grazing-incidence wide-angle X-ray scattering (GIWAXS) and spectroscopic ellipsometry (SE). We focus on a blend of the polymer poly[*N*-9′-heptadecanyl-2,7-carbazole-*alt*-5,5-(4′,7′-di-2-thienyl-2′,1′,3′-benzothiadiazole)] (PCDTBT) with the functionalised fullerene [6,6]-phenyl-C71-butyric acid methyl ester ($PC_{70}BM$). When processed into an OPV device, a PCDTBT:$PC_{70}BM$ blend has been shown to exhibit high power conversion efficiencies and internal quantum efficiencies[31] and promising operational stability.[6] For comparative purposes, we also explore the drying dynamics of a number of other amorphous polymer:fullerene blends to determine any generality in the aggregation of $PC_{70}BM$ during the film formation process. Our measurements show that in the samples studied, film drying is dominated by the initial coalescence of $PC_{70}BM$ molecules that leads to the formation of nanoscale aggregates. For the PCDTBT blend, an apparent delay in Bragg scatter from the PCDTBT-rich phase of the film suggests that $PC_{70}BM$ aggregation occurs before ordering of the polymer-rich phase of the film.

2. Results and Discussion

The combination of GIWAXS and SE permits the degree of molecular order within a polymer:fullerene film, its thickness and its complete refractive index to be determined simultaneously as it dries. In particular, modelling of the SE data at wavelengths below the optical band-gap of the blend film is a powerful technique to determine film thickness. We can use this data to extract the relative composition of the film (i.e. its solid concentration) as solvent evaporates from the solution and the film proceeds towards a dry state. Our experimental methods are described in detail in our earlier work.[24] Briefly however, a bar-coater housed within a sample environment chamber is placed in the path of an X-ray beam, with the beam directed at grazing incidence to the centre of the sample substrate. An ellipsometer is placed so that light from the instrument illuminates the centre of the sample substrate and overlaps with part of the film that is probed by the X-ray beam. This setup is shown schematically in **Figure 1**. Blend solutions were dispensed using a syringe pump, and then cast across the sample substrate using the bar coater. The start of the solution delivery acts as a trigger for simultaneous acquisition of GIWAXS and SE data, which are recorded as the film dries.

2.1. Drying Dynamics of PCDTBT:$PC_{70}BM$

We first discuss the development of structure in blend films of PCDTBT:$PC_{70}BM$ (1:4 wt%) cast from 1,2-dichlorobenzene (DCB). In **Figure 2**(a), we present the thickness evolution of the film recorded during the drying process. The solid content of the film, as calculated from the ratio of the film thickness to the dry film thickness, is shown in Figure 2(b). For the majority of the drying time, the drying rate is constant and likely corresponds to the unimpeded evaporation of solvent molecules.[22,24] An abrupt reduction in solvent loss rate is found to occur at 225 s, corresponding to a solid concentration of approximately 90 wt%. This process is then followed by a relatively slow convergence to a dry film. We note that the sharp reduction in solvent loss rate determined here occurs at a much higher solid concentration than occurs in blends of P3HT:PCBM, (~50%) in which efficient photocurrent generation is maximised at a P3HT:PCBM film composition of 1:0.8 wt%.[24] Variations in the solid solubility

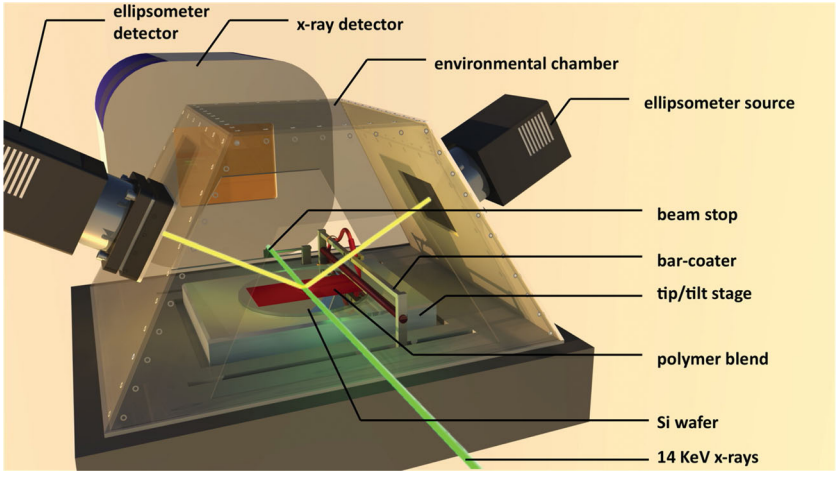

Figure 1. Schematic illustration of the experimental setup with principle components identified.

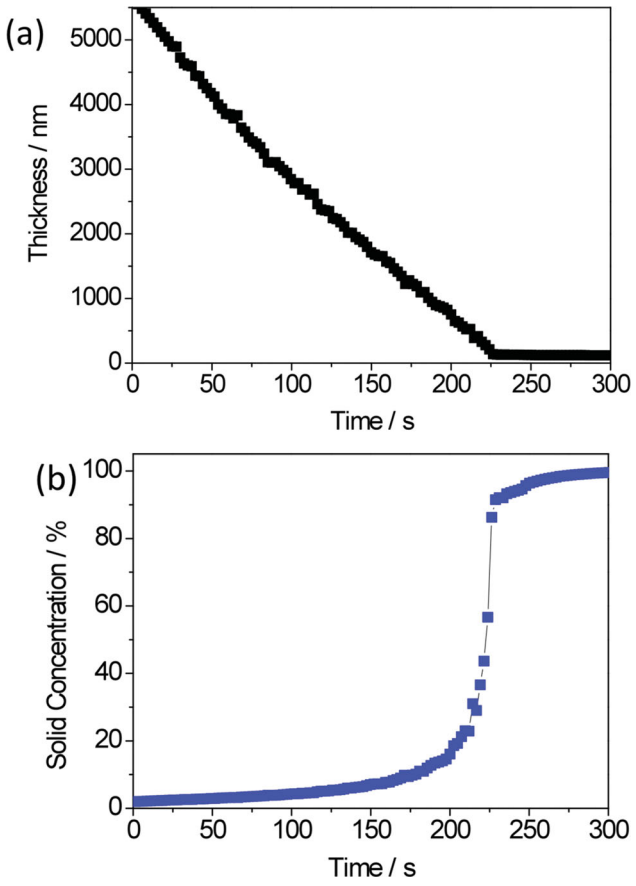

Figure 2. Evolution in film thickness (a) and solid concentration (b) of a PCDTBT:$PC_{70}BM$ 1:4 wt% blend during solution casting. Solid concentration is determined from the thickness of the film relative to the final film thickness.

in the casting solvent, or in the relative ability of the blend to 'trap' solvent during film casting, may provide an explanation for this difference.

To develop our understanding of morphology formation, we have used GIWAXS to study the evolution in film structure at a molecular level during film casting. Such measurements were performed simultaneously with the SE data that is presented in Figure 2. In **Figure 3** we present 2D X-ray scattering patterns recorded at four distinct stages during the drying process alongside the relative solid content in the film at that time, as inferred from SE. Initially, the dominant source of X-ray scatter (at Q = 1.15 and 1.82 $Å^{-1}$) is from DCB solvent molecules.[22,32] As the solvent content reduces, the relative intensity of these diffuse solvent scattering rings decreases. At approximately 230 s into the film drying process (corresponding to the point where the relative solid content of the film has substantially increased), X-ray scatter from PCDTBT and $PC_{70}BM$ begins to dominate (see Figure 3(c)). In the final image, (Figure 3(d)) the film is considered to be essentially dry and Bragg scatter comes primarily from $PC_{70}BM$, as indicated by the relatively broad and intense ring at Q = 1.34 $Å^{-1}$. The presence of a broad symmetric ring at this Q-value indicates a random orientation of small fullerene domains within the film.[33]

In **Figure 4**(a) we plot radial line profiles from each GIWAXS measurement as a function of time. This permits the evolution of a film dominated by solvent-scatter to that of solid-dominated scatter during the film drying process to be detailed. Specifically, the transition from solvent to fullerene dominated X-ray scatter is evidenced by a gradual transition from a scattering peak located at 1.15 $Å^{-1}$ (a signal dominated by solvent scatter) to a peak at 1.34 $Å^{-1}$ (corresponding to aggregated $PC_{70}BM$). For completeness, we have also recorded the evolution in X-ray scatter from a pure PCDTBT film during the casting process, as shown in Figure 4(b). Here we find no shift in the position of the solvent scattering rings during the drying process. Clearly the peak Q-value of the scattering feature that apparently moves across the Q range 1.1 – 1.4 $Å^{-1}$ in the polymer:fullerene blend is determined by the relative contribution of scattering from both the solvent and $PC_{70}BM$ to the overall signal. We believe therefore that the shift in Q-value of this composite X-ray scattering feature reflects a relative increase in the population of nanoscale $PC_{70}BM$ aggregates within the drying film; a process mediated by the evaporation of solvent molecules. Once the film is dry, the broad nature of the $PC_{70}BM$ scattering rings indicates that the degree of long-range order in the $PC_{70}BM$ phases of the blend film is relatively low. This most likely results from strong polymer-fullerene molecular interactions that inhibit bulk crystallisation of the fullerene. We can calculate the molecular coherence length L of the $PC_{70}BM$-rich phase of the blend film using the expression $L = 2\pi/\Delta$, where Δ corresponds to the full-width at half-maximum (FWHM) of the Bragg scattering peak. Using this approach we determine a coherence length for the $PC_{70}BM$ scattering feature at Q = 1.34 $Å^{-1}$ of L = 21.0 ± 1.0 Å.

To determine the onset time at which $PC_{70}BM$ aggregates develop, it is necessary to decompose each scattering pattern into a series of peaks that can be used to quantify the relative contribution of both solvent and solid X-ray scatter, in addition to any contribution from the background (see the Experimental Section for details). In this analysis, we do not permit the positions or widths of the peaks to vary; an assumption we believe justifable owing to the amorphous nature of the sample and apparent absence of long-range order in the dry film, as determined by the coherence length calculation.

In Figure 4(c), we plot the peak intensities of the two solvent peaks (centred at Q = 1.15 $Å^{-1}$ and Q = 1.81 $Å^{-1}$) and the dominant $PC_{70}BM$ peak (centred at Q = 1.34 $Å^{-1}$). An example of the deconvolution of an X-ray scattering profile into its different components is shown in the Supporting Information, Figure S1. For simplicity, the evolution of the relatively low scattering intensity $PC_{70}BM$ peak at Q = 1.94 $Å^{-1}$ is omitted from our discussion. In Figure 4(c), it can be seen that the first 50s of film formation is characterised by a relatively gradual reduction in X-ray scatter from the solvent; a result consistent with the reduction in film thickness as determined by SE. Over this timescale no significant change in X-ray scatter from $PC_{70}BM$ is found. Beyond approximately 50 s however, it can be seen that the intensity of the $PC_{70}BM$ X-ray scattering peak undergoes a relative increase, a process that continues in an approximately linear fashion until 240 s into the film drying process. This intermediate time period is also characterised by a progressively faster reduction in the intensity of X-ray scatter from

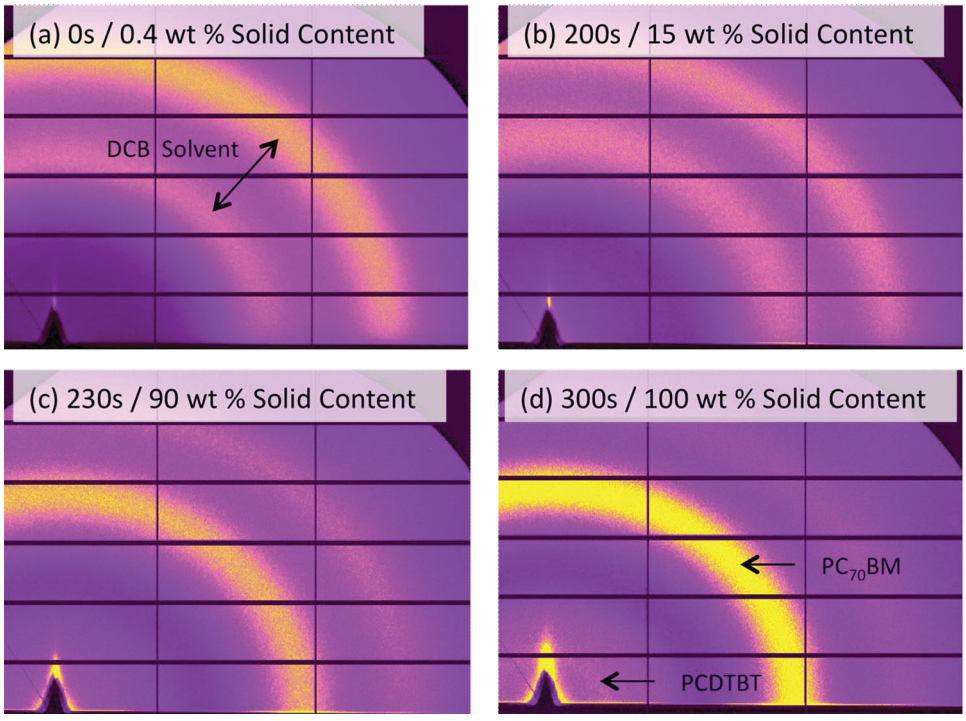

Figure 3. 2D GIWAXS images of a PCDTBT:$PC_{70}BM$ 1:4 wt% blend during solution casting: In each frame (a–d) the approximate solid concentrations taken from the SE measurement is shown.

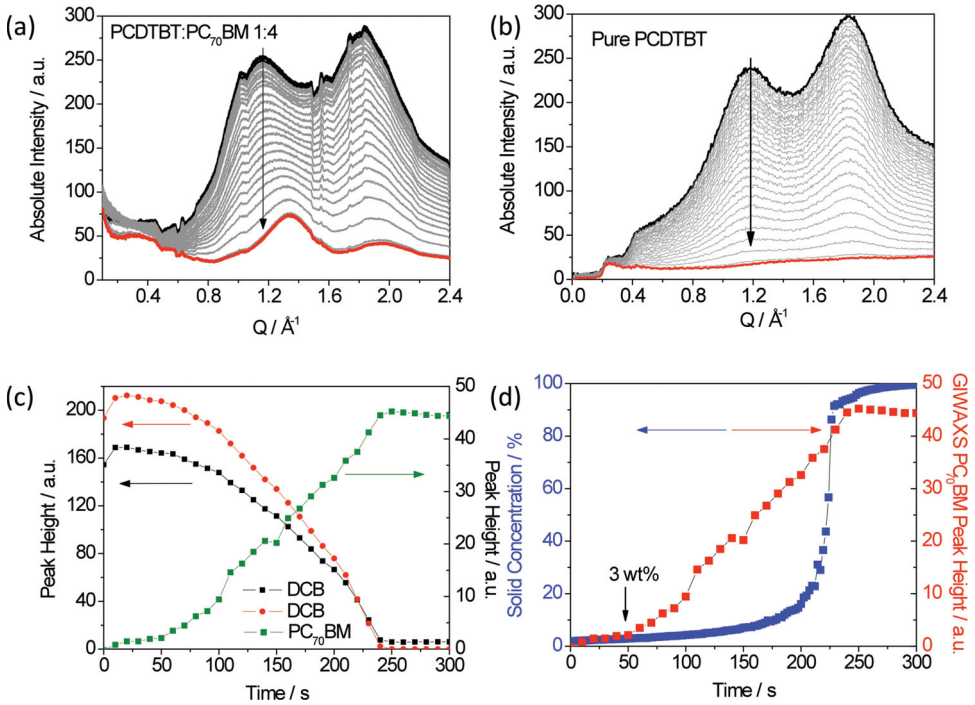

Figure 4. (a) Radial line profiles of the X-ray scattering intensity obtained from each 2D GIWAXS image over the course of solution casting. Part (b) shows X-ray scattering profiles of a pure PCDTBT film after solution casting. In both figures the arrows indicate the direction of increasing time. Black and red lines correspond to the initial and final scattering patterns respectively. In part (c) the peak height of each function used to describe the contribution of X-ray scatter from both solvent and $PC_{70}BM$ (peak at Q =1.34 $Å^{-1}$ only) to the overall X-ray scattering profile is presented as a function of time. Data presented in red corresponds to the dynamics of solvent X-ray scatter at Q =1.81 $Å^{-1}$ and data presented in black corresponds to the dynamics of solvent X-ray scatter at Q = 1.15 $Å^{-1}$. In part (d), the evolution in X-ray scatter corresponding to aggregated $PC_{70}BM$ (Q = 1.34 $Å^{-1}$) is shown alongside the solid content evolution of the drying film, as determined by SE.

solvent within the film. Beyond 240 s no discernable changes in the intensity of X-ray scattering from any feature is observed.

In Figure 4(d) we compare the time-dependent change in $PC_{70}BM$ scattering intensity with changes in film solid concentration derived from SE measurements. From this comparison a significant difference in dynamics in the increase of $PC_{70}BM$ X-ray scatter and the increase in film solid concentration can be seen. Specifically, by comparing the onset time for fullerene aggregation (~50 s) with the evolution in film solid concentration we conclude that the fullerene component of the film starts to aggregate when the blend solid concentration reaches approximately 3 ± 2 wt%; a value far below the threshold concentration at which there is a significant reduction in the solvent loss rate. This value has been conservatively estimated from the data by identifying the point at which the X-ray scattering intensity from $PC_{70}BM$ starts to increase. We note that a study of the drying dynamics of P3HT:PCBM by Schmidt-Hansberg et al. estimated the solubility of PCBM in DCB solvent to be 3 wt% at 25 °C.[22] It appears therefore that once the solubility limit of $PC_{70}BM$ in DCB has been reached, the film undergoes a progressive transition from a casting solution containing well-dissolved solids to one in which the solid content begins to precipitate. At around 240 s (corresponding to a film solid concentration of 94 wt%), the rate of change in film composition and morphology slows, with the structures formed rapidly approaching their final conformation.

We now discuss the formation of the PCDTBT rich phase in the blend film during casting. Typically, as-cast films of PCDTBT are relatively amorphous, having a characteristic lamella spacing of approximately 20.9 Å and a π–π stacking distance of approximately 4.4 Å.[34–36] In Figure 4(a) it can be seen that a broad peak centred at Q = 0.32 $Å^{-1}$ (d = 19.6 Å) is present in the X-ray scattering pattern corresponding to the dry film. Note that in the out-of-plane direction, this feature is found to coincide with an X-ray flare above the beamstop. We identify scattering at this Q value as originating from PCDTBT, specifically first order scattering between neighbouring chains along the lamella direction.[34–36] Here, the weak signal intensity reflects both the semi-amorphous nature of the polymer and its low concentration (20 wt%) in the blend film.

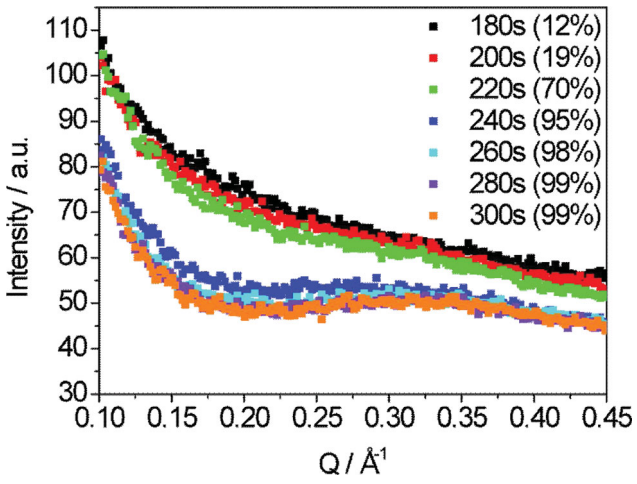

Figure 5. Radial line profiles of X-ray scatter at relatively low Q presented as a function of time, highlighting the onset of weak X-ray scatter from PCDTBT. Values in parentheses correspond to the average solid concentration of the film over the intergration time of each X-ray measurement.

From Figure 4(a) it is apparent that X-ray scatter from $PC_{70}BM$ molecules is already relatively pronounced by the time at which X-ray scatter from the PCDTBT-rich phase of the film is first resolved. This is clarified in **Figure 5**, where we detail X-ray scatter over the Q-range 0.1–0.45 $Å^{-1}$ from the sample over the time range 180–300 s after solution casting. Here, it can be seen that the transition towards a resolvable X-ray scattering feature above the measured background only occurs after 220 s. The delayed onset time for X-ray scatter from PCDTBT, compared to X-ray scattering from $PC_{70}BM$ (See Figure 4(c)) suggests that ordering of the polymer and fullerene start at different times, with weak ordering between polymer chains only occurring towards the end of the drying process and significantly later than the onset of fullerene aggregation. We speculate therefore that regions rich in PCDTBT may arrange themselves around fullerene aggregates that have previously formed in solution; a process that we illustrate schematically in **Figure 6**. This

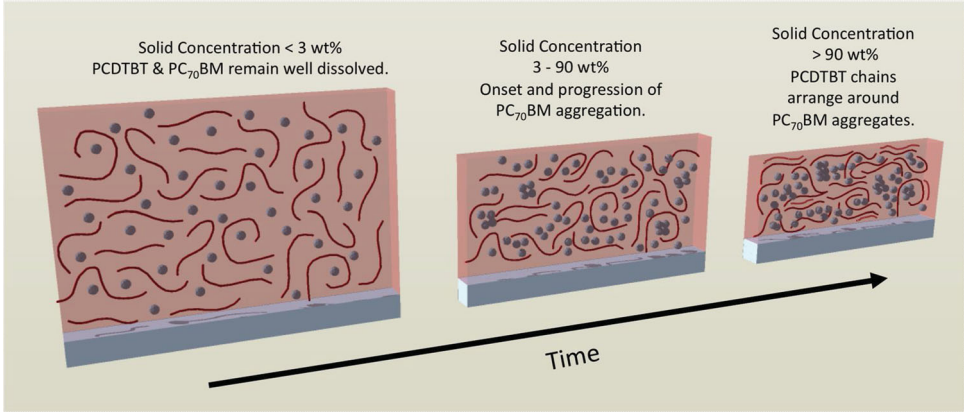

Figure 6. Proposed model of film formation for a PCDTBT:$PC_{70}BM$ 1:4 wt% blend during solution casting. We highlight the three key stages in the process determined by our measurements. At early times (a), the film contains a high solvent fraction and its components (polymer and fullerene molecules) undergo very little self-interaction. As the solid concentration reaches approximately 3% (b), the solubility limit of $PC_{70}BM$ is reached; a process which initiates its precipitation from solution and thus aggregation. In the final stage of film drying (c), the PCDTBT polymer undergoes weak lamella ordering.

behaviour appears to be different from the drying kinetics of semi-crystalline polymer:fullerene blend films having a composition optimised for OPV device operation (e.g. P3HT:PCBM). In such systems, the fullerene concentration is typically lower than that of the polymer, with ordering in the polymer phase of the film occuring before fullerene aggregation.[22] It is important to acknowledge however that by characterising the formation of film nanostucture via GIWAXS, we are unable to quantify the exact distribution of $PC_{70}BM$ molecules between pure and mixed phases. We note that alternative techniques, such as neutron reflectivity[37] and resonant soft X-ray scattering,[38] are better suited for this task as they can generate a larger contrast variation between the polymer and fullerene components.

2.2. Drying Dynamics of PCDTBT-8, MEH-PPV, and P3HT:$PC_{70}BM$ Blends

To determine whether the process of fullerene aggregation in a PCDTBT:$PC_{70}BM$ blend displays any general behaviour, we now discuss the drying kinetics of a range of different polymer:fullerene blend films, in which each blend is composed of the same high weight concentration (80 wt%) of $PC_{70}BM$. This is plotted in **Figure 7**, where we show the evolution in X-ray scatter from PCDTBT-8:$PC_{70}BM$,[39] MEH-PPV:$PC_{70}BM$ and P3HT:$PC_{70}BM$ blend films during solution casting, following peak decomposition analysis of the data. We note that thin-film blends of PCDTBT-8:$PC_{70}BM$ and MEH-PPV:$PC_{70}BM$ display the highest photovoltaic efficiency in OPV devices when the active layer composition is approximately 1:4 wt%,[39,40] a value similar to that of a blend of PCDTBT:$PC_{70}BM$. In contrast, the inclusion of a P3HT:$PC_{70}BM$ blend film presents an opportunity to compare a blend film in which the solubility of $PC_{70}BM$ in the polymer is lower than that of PCDTBT:$PC_{70}BM$.[37,41,42]

In Figure 7, it can be seen that the evolution in X-ray scattering intensity in each sample for both solvent and $PC_{70}BM$ are broadly similar to the dynamics of PCDTBT:$PC_{70}BM$; specificially an increase in scattering intensity from $PC_{70}BM$ aggregates is delayed with respect to the initial casting of the film. Note, the exact time for the onset of rapid increase in the solid concentration of the PCDTBT-8:$PC_{70}BM$ film appears to occur at an earlier time after film casting than is observed in all the other blends studied. We do not believe this represents a systematic difference in the behaviour of this particular blend. Rather, it is likely to result from the fact that the film cast in this experiment was slightly thinner than those cast in our other measurements. This difference most probably arose from variations in the bar-coating process.

In Figure 7(c) we present the X-ray drying kinetics of a thin-film blend of P3HT:$PC_{70}BM$. Although P3HT is a semi-crystalline polymer, its drying dynamics in a blend film containing a high wt% of $PC_{70}BM$ are nevertheless qualitatively similar to the other amorphous polymers:$PC_{70}BM$ blends. Note, we do not evidence a significant degree of order within the polymer phase of the film; GIWAXS scatter from the fully dry film is comparable to a blend film of RRa-P3HT:$PC_{70}BM$ with identical film composition (See Supporting Information), suggesting the polymer rich phase of the P3HT blend film is largely amorphous. This is supported by modelling of the optical extinction coefficient

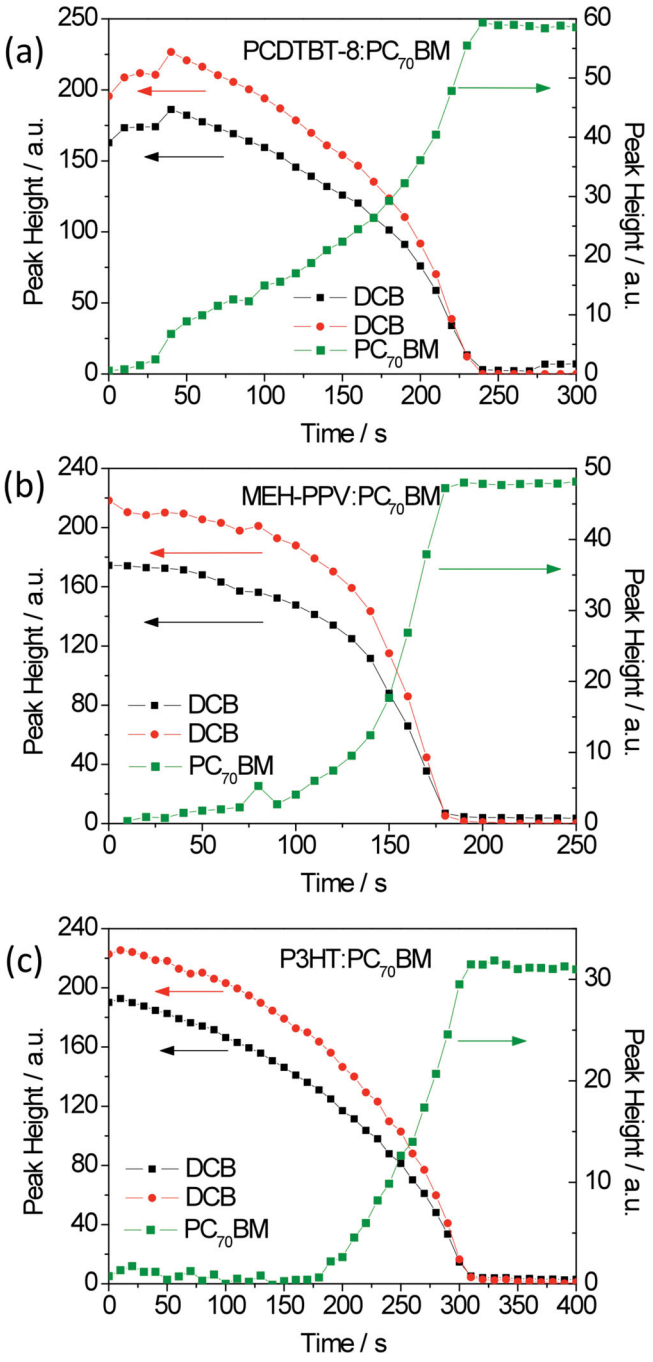

Figure 7. Evolution in X-ray scattering intensity from the casting solvent and aggregated $PC_{70}BM$ (peak at Q = 1.34 $Å^{-1}$ only) for blend films of (a) PCDTBT-8:$PC_{70}BM$, (b) MEH-PPV:$PC_{70}BM$, (c) RR-P3HT:$PC_{70}BM$. The fullerene composition for each blend is 80 wt%. Data presented in red corresponds to the dynamics of solvent X-ray scatter at Q =1.81 $Å^{-1}$ and data presented in black corresponds to the dynamics of solvent X-ray scatter at Q = 1.15 $Å^{-1}$.

spectrum for the P3HT:$PC_{70}BM$ blend film (obtained from SE measurements), which does not evidence any vibronic structure typical of semi-crystalline P3HT (See Supporting Information). These results are consistent with earlier work on P3HT:PCBM blend films that have shown the ability of fullerene molecules to

disrupt polymer crystallisation when present at sufficiently high weight concentration within the blend film.[43]

To rationalise the changes in X-ray scattering intensity from $PC_{70}BM$ molecules after the onset of coalescence, we again compare the dynamics of film drying as observed using GIWAXS with simultaneous SE measurements. This is shown in **Figure 8**, where we plot the intensity of X-ray scattering from aggregated $PC_{70}BM$ against the solid concentration in the film as determined from SE. Data is again plotted for the three different polymer:$PC_{70}BM$ blends introduced earlier.

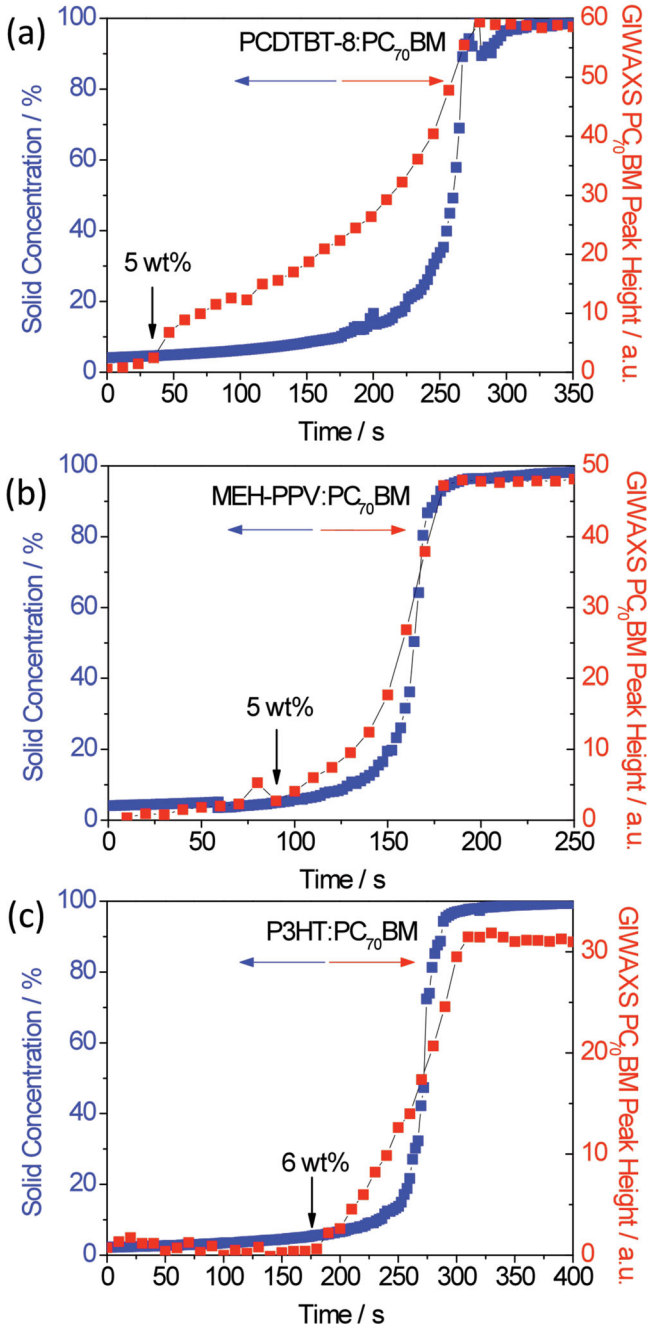

Figure 8. Comparison between the evolution of X-ray scattering from aggregated $PC_{70}BM$ and film solid concentration (determined from SE measurements) during solution casting. (a) PCDTBT-8:$PC_{70}BM$, (b) MEH-PPV:$PC_{70}BM$, (c) P3HT:$PC_{70}BM$. The fullerene composition for each blend is 80 wt%.

It can be seen that the early-time kinetics of $PC_{70}BM$ X-ray scattering intensity is characteristically similar to the drying dynamics of PCDTBT:$PC_{70}BM$. The total solid concentration within each sample, beyond which $PC_{70}BM$ is believed to precipitate from solution, is estimated as 5 ± 2 wt%, 5 ± 2 wt% and 6 ± 2 wt% for the PCDTBT-8, MEH-PPV and P3HT blend films respectively. The solid concentration corresponding to the onset of the 'plateau' region of maximum $PC_{70}BM$ X-ray scattering intensity is 94 wt%, 92 wt% and 98% for the PCDTBT-8, MEH-PPV and P3HT blend films respectively. Note however that the rate of change in X-ray scattering intensity from aggregated $PC_{70}BM$ in each of these systems is different to that of the PCDTBT:$PC_{70}BM$ blend. We speculate that differences in polymer-fullerene molecular interactions that determine the nanoscale morphology in each blend may account for such variation.

3. Conclusions

Using a combination of GIWAXS and SE, the formation of structure in solution cast films of PCDTBT:$PC_{70}BM$ (1:4 wt%) has been investigated with a number of stages identified. We find that coalescence of fullerene molecules occurs in solution once the solubility limit of $PC_{70}BM$ in the casting solvent is reached (here determined as 3 ± 2 wt%). The subsequent growth in the intensity of X-ray scatter from fullerene aggregates within the film occurs in a linear manner until the film is almost dry. A delay in X-ray scatter associated with the polymer rich phase of the blend suggests that weak ordering of the fullerene component precedes ordering within the PCDTBT-rich phase of the film. This behaviour is distinctly different to the dynamics of semi-crystalline polymer:fullerene blend films that have been optimised for OPV application, where the fullerene concentration is generally lower. For these systems, previous work has shown that ordering in the polymer phase occurs first. We have also monitored the drying dynamics of a range of amorphous polymer:$PC_{70}BM$ blends, each containing a relatively high concentration of fullerene and have identified in each case a similar threshold solid concentration beyond which fullerene aggregation occurs (between (5 ± 2) & (6 ± 2) wt%). It appears therefore that the drying dynamics in amorphous conjugated polymer:fullerene films containing a high weight fraction (80 wt%) of fullerenes show very similar behaviour, which appears largely independent of the exact structure of the polymer. This apparent generality most likely results from the fact that the concentration of the polymer present in the films studied is relatively low (20 wt%). At higher polymer concentrations, variations in film drying dynamics will be dependent on the nature of the polymer – for example in its ability to self-organise and trap solvent. Our observations thus provide partial insight into the development of structure in technologically relevant polymer:fullerene blends that contain a high fullerene loading and potentially assist the future optimisation and understanding of structure formation in this category of materials.

4. Experimental Section

Materials and Solution Preparation: PCDTBT (M_w 36 700, M_n 17 000) and PCDTBT-8 (M_w 34 800, M_n 14 700) were synthesised according to previously reported methods.[31]9 Regio-random P3HT and MEH-PPV were purchased from Sigma Aldrich (Product Numbers 510823 and 541443 respectively). Regio-regular P3HT (Rieke 4002-E) and $PC_{70}BM$ (95% purity) were purchased from Ossila Ltd. All materials were used as received. All blends were prepared in 1,2-dichlorobenzene solvent at a total solid concentration of 4 mg/ml. Solutions were held at 70 °C for 18 h before use to encourage full dissolution of the solid content.

Sample Preparation: Thin-films were cast using a bar-coating technique, where a wire-bound bar was translated across the surface of silicon/native oxide substrate after the solution was dispensed in front of the bar using a syringe pump. The initial thickness of the wet film is nominally 4 µm. Typically, 40 µL of polymer:$PC_{70}BM$ solution was dispensed for film casting with the bar moving across the substrate at a speed of 20 mm/s. Once cast, the film was permitted to dry at room temperature; a process that took around 300 s.

In-situ Measurements: Ellipsometry measurements were performed using a spectroscopic ellipsometer (M2000v, J.A. Woollam Co., USA) with an incidence angle set to 70° from vertical. Dynamic data were recorded every 2.4 s. For data analysis, the polymer:$PC_{70}BM$ blends were regarded as a homogeneous layer with film thickness modelled using a Cauchy model over the wavelength range 750 to 1000 nm.[24]

Two-dimensional grazing-incidence wide-angle X-ray scattering measurements (GIWAXS) were carried out at the I22 beam-station at the Diamond Light Source (Didcot, UK). Here, a 14 keV energy X-ray beam was incident on the sample surface at a grazing incidence angle of 0.16°. Data was recorded with an integration time of 10 s with zero delay between each frame. The sample chamber contained a slight overpressure of helium gas to reduce background X-ray scatter. Data was calibrated using silver behenate and 1D scattering profiles were obtained using the DAWN software package (http://www.dawnsci.org). Radial line profiles were calculated over a 20° angular range centred at 60° away from the sample normal. To determine the kinetics of fullerene aggregation in each system, each solvent and $PC_{70}BM$ scattering feature was modeled using a single Gaussian peak. The first scattering pattern in each time series was used to characterise the positions and widths of the two functions corresponding to solvent scatter. Similarly, the final scattering pattern in each time series were used to characterise the two functions corresponding to $PC_{70}BM$ scatter. Only the intensity of each Gaussian peak was permitted to vary in the decomposition of each scattering pattern. For each sample, a sum of two exponential functions were used to characterise background X-ray scatter.[38] The quality of each fit (quantifed by a R^2 analysis) was above 0.98 for all datasets.

Supporting Information

Supporting Information is available from the Wiley Online Library or from the author.

Acknowledgements

We thank EPSRC for funding via grants EP/I028641/1, EP/J017361/1 and EP/G062404/1. AJP thanks King Abdulaziz University for financial support via grant no. D-004/431. We thank the Diamond Light Source for support through the MT1203 beamtime allocation, and Diamond staff for their help.

Received: June 5, 2013
Revised: June 28, 2013
Published online: October 2, 2013

[1] M. Helgesen, R. Sondergaard, F. C. Krebs, *J. Mater. Chem.* **2010**, *20*, 36.
[2] F. C. Krebs, *Solar Energy Mater. Solar Cells* **2009**, *93*, 394.
[3] F. C. Krebs, M. Jorgensen, K. Norrman, O. Hagemann, J. Alstrup, T. D. Nielsen, J. Fyenbo, K. Larsen, J. Kristensen, *Solar Energy Mater. Solar Cells* **2009**, *93*, 422.
[4] L. T. Dou, J. B. You, J. Yang, C. C. Chen, Y. J. He, S. Murase, T. Moriarty, K. Emery, G. Li, Y. Yang, *Nat. Photonics* **2012**, *6*, 180.
[5] Z. C. He, C. M. Zhong, S. J. Su, M. Xu, H. B. Wu, Y. Cao, *Nat. Photonics* **2012**, *6*, 591.
[6] C. H. Peters, I. T. Sachs-Quintana, J. P. Kastrop, S. Beaupre, M. Leclerc, M. D. McGehee, *Adv. Energy Mater.* **2011**, *1*, 491.
[7] C. J. Brabec, S. Gowrisanker, J. J. M. Halls, D. Laird, S. J. Jia, S. P. Williams, *Adv. Mater.* **2010**, *22*, 3839.
[8] B. Azzopardi, C. J. M. Emmott, A. Urbina, F. C. Krebs, J. Mutale, J. Nelson, *Energy Environ. Sci.* **2011**, *4*, 3741.
[9] X. Yang, J. Loos, *Macromolecules* **2007**, *40*, 1353.
[10] M. Campoy-Quiles, T. Ferenczi, T. Agostinelli, P. G. Etchegoin, Y. Kim, T. D. Anthopoulos, P. N. Stavrinou, D. D. C. Bradley, J. Nelson, *Nature Mater.* **2008**, *7*, 158.
[11] M. A. Brady, G. M. Su, M. L. Chabinyc, *Soft Matter* **2011**, *7*, 11065.
[12] M. A. Ruderer, P. Muller-Buschbaum, *Soft Matter* **2011**, *7*, 5482.
[13] W. Yin, M. Dadmun, *ACS Nano* **2011**, *5*, 4756.
[14] B. A. Collins, J. R. Tumbleston, H. Ade, *J. Phys. Chem. Lett.* **2011**, *2*, 3135.
[15] N. D. Treat, M. A. Brady, G. Smith, M. F. Toney, E. J. Kramer, C. J. Hawker, M. L. Chabinyc, *Adv. Energy Mater.* **2011**, *1*, 82.
[16] A. J. Parnell, A. J. Cadby, O. O. Mykhaylyk, A. D. F. Dunbar, P. E. Hopkinson, A. M. Donald, R. A. L. Jones, *Macromolecules* **2011**, *44*, 6503.
[17] F. Liu, Y. Gu, C. Wang, W. Zhao, D. Chen, A. L. Briseno, T. P. Russell, *Adv. Mater.* **2012**, *24*, 3947.
[18] Y. Gu, C. Wang, T. P. Russell, *Adv. Energy Mater.* **2012**, *2*, 683.
[19] W. R. Wu, U. S. Jeng, C. J. Su, K. H. Wei, M. S. Su, M. Y. Chiu, C. Y. Chen, W. B. Su, C. H. Su, A. C. Su, *ACS Nano* **2011**, *5*, 6233.
[20] T. Wang, A. J. Pearson, D. G. Lidzey, R. A. L. Jones, *Adv. Funct. Mater.* **2011**, *21*, 1383.
[21] J. T. Rogers, K. Schmidt, M. F. Toney, G. C. Bazan, E. J. Kramer, *J. Am. Chem. Soc.* **2012**, *134*, 2884.
[22] B. Schmidt-Hansberg, M. Sanyal, M. F. G. Klein, M. Pfaff, N. Schnabel, S. Jaiser, A. Vorobiev, E. Muller, A. Colsmann, P. Scharfer, D. Gerthsen, U. Lemmer, E. Barrena, W. Schabel, *ACS Nano* **2011**, *5*, 8579.
[23] M. Sanyal, B. Schmidt-Hansberg, M. F. G. Klein, A. Colsmann, C. Munuera, A. Vorobiev, U. Lemmer, W. Schabel, H. Dosch, E. Barrena, *Adv. Energy Mater.* **2011**, *1*, 363.
[24] T. Wang, A. D. F. Dunbar, P. A. Staniec, A. J. Pearson, P. E. Hopkinson, J. E. MacDonald, S. Lilliu, C. Pizzey, N. J. Terrill, A. M. Donald, A. J. Ryan, R. A. L. Jones, D. G. Lidzey, *Soft Matter* **2010**, *6*, 4128.
[25] E. Verploegen, C. E. Miller, K. Schmidt, Z. N. Bao, M. F. Toney, *Chem. Mater.* **2012**, *24*, 3923.
[26] A. J. Pearson, T. Wang, D. G. Lidzey, *Rep. Prog. Phys.* **2013**, 76, 022501.
[27] F. Liu, Y. Gu, J. W. Jung, W. H. Jo, T. P. Russell, *J. Polym. Sci. Pol. Phys.* **2012**, *50*, 1018.
[28] Y. Vaynzof, D. Kabra, L. H. Zhao, L. L. Chua, U. Steiner, R. H. Friend, *ACS Nano* **2011**, *5*, 329.
[29] B. Watts, W. J. Belcher, L. Thomsen, H. Ade, P. C. Dastoor, *Macromolecules* **2009**, *42*, 8392.
[30] D. Chen, F. Liu, C. Wang, A. Nakahara, T. P. Russell, *Nano Lett.* **2011**, *11*, 2071.
[31] S. H. Park, A. Roy, S. Beaupre, S. Cho, N. Coates, J. S. Moon, D. Moses, M. Leclerc, K. Lee, A. J. Heeger, *Nat. Photonics* **2009**, *3*, 297.

[32] B. Schmidt-Hansberg, M. F. G. Klein, M. Sanyal, F. Buss, G. Q. G. de Medeiros, C. Munuera, A. Vorobiev, A. Colsmann, P. Scharfer, U. Lemmer, E. Barrena, W. Schabel, *Macromolecules* **2012**, *45*, 7948.

[33] Y. Kim, J. Nelson, T. Zhang, S. Cook, J. R. Durrant, H. Kim, J. Park, M. Shin, S. Nam, M. Heeney, I. McCulloch, C. S. Ha, D. D. C. Bradley, *ACS Nano* **2009**, *3*, 2557.

[34] X. H. Lu, H. Hlaing, D. S. Germack, J. Peet, W. H. Jo, D. Andrienko, K. Kremer, B. M. Ocko, *Nat. Commun.* **2012**, *3*, 795.

[35] N. Blouin, A. Michaud, D. Gendron, S. Wakim, E. Blair, R. Neagu-Plesu, M. Belletete, G. Durocher, Y. Tao, M. Leclerc, *J. Am. Chem. Soc.* **2008**, *130*, 732.

[36] P. A. Staniec, A. J. Parnell, A. D. F. Dunbar, H. Yi, A. J. Pearson, T. Wang, P. E. Hopkinson, C. Kinane, R. M. Dalgliesh, A. M. Donald, A. J. Ryan, A. Iraqi, R. A. L. Jones, D. G. Lidzey, *Adv. Energy Mater.* **2011**, *1*, 499.

[37] H. P. Chen, R. Hegde, J. Browning, M. D. Dadmun, *Phys. Chem. Chem. Phys.* **2012**, *14*, 5635.

[38] B. A. Collins, Z. Li, J. R. Tumbleston, E. Gann, C. R. McNeill, H. Ade, *Adv. Energy Mater.* **2013**, *3*, 65.

[39] H. Yi, S. Al-Faifi, A. Iraqi, D. C. Watters, J. Kingsley, D. G. Lidzey, *J. Mater. Chem.* **2011**, *21*, 13649.

[40] G. Yu, J. Gao, J. C. Hummelen, F. Wudl, A. J. Heeger, *Science* **1995**, *270*, 1789.

[41] N. C. Cates, R. Gysel, J. E. P. Dahl, A. Sellinger, M. D. McGehee, *Chem. Mater.* **2010**, *22*, 3543.

[42] T. Wang, A. J. Pearson, A. D. F. Dunbar, P. A. Staniec, D. C. Watters, H. Yi, A. J. Ryan, R. A. L. Jones, A. Iraqi, D. G. Lidzey, *Adv. Funct. Mater.* **2012**, *22*, 1399.

[43] P. E. Hopkinson, P. A. Staniec, A. J. Pearson, A. D. F. Dunbar, T. Wang, A. J. Ryan, R. A. L. Jones, D. G. Lidzey, A. M. Donald, *Macromolecules* **2011**, *44*, 2908.

